CrossMark

Single-pulse Emission Variation of Two Pulsars Discovered by FAST

Ziping Guo[1,2], Zhigang Wen[1,2,3], Jianping Yuan[1,2,3], Feifei Kou[1,2], Qingdong Wu[1,2], Na Wang[1,2,3], Weiwei Zhu[4], Di Li[2,4,7], Mengyao Xue[4], Pei Wang[4,8], Chenchen Miao[4], De Zhao[1,2], Yue Hu[5], Wenming Yan[1,2,3], Jiarui Niu[4], Rukiye Rejep[4], and Zhipeng Huang[6]

[1] Xinjiang Astronomical Observatory, Chinese Academy of Sciences, Urumqi 830011, China; yuanjp@xao.ac.cn
[2] University of Chinese Academy of Sciences, Beijing 100049, China
[3] Xinjiang Key Laboratory of Radio Astrophysics, Urumqi 830011, China
[4] National Astronomical Observatories, Chinese Academy of Sciences, Beijing 100101, China
[5] National Time Service Center (NTSC) of the Chinese Academy of Sciences (CAS), Xi'an 710600, China
[6] Shanghai Astronomical Observatory, Chinese Academy of Sciences, Shanghai 200030, China
[7] Zhejiang Lab, Hangzhou 311121, China
[8] Institute for Frontiers in Astronomy and Astrophysics, Beijing Normal University, Beijing 102206, China

Abstract

We investigate the single-pulse emission variations of two pulsars, PSRs J0211+4235 and J0553+4111, observed with the Five-hundred-meter Aperture Spherical radio Telescope at the 1.25 GHz central frequency. The observation sessions span from 2020 December to 2021 July, with 21 and 22 observations for them respectively. The integrated pulse profile of PSR J0211+4235 shows that there is a weak pulse component following the main component, and PSR J0553+4111 displays a bimodal profile with a bridge component in the middle. PSR J0211 +4235 presents significant nulling phenomenon with nulling duration lasting from 2 to 115 pulses and burst duration lasting from 2 to 113 pulses. The NF of each observation is determined to be 45%–55%. No emission greater than three σ is found in the mean integrated profile of all nulling pulses. In most cases, the pulse energy changes abruptly during the transition from null to burst, while in the transition from burst to null there are two trends: abrupt and gradual. We find that the nulling phenomenon of PSR J0211+4235 is periodic by the Fourier transform of the null and burst state. In addition, the single-pulse modulation characteristics of these two pulsars are investigated, and the distributions of modulation index, LRFS and 2DFS are analyzed with PSRSALSA. The left peak of PSR J0553+4111 has intensity modulation. Finally, the polarization properties of these two pulsars are obtained through polarization calibration, and their characteristics are analyzed. The possible physical mechanisms of these phenomena are discussed.

Key words: (stars:) pulsars: general – (stars:) pulsars: individual (PSR J0211+4235, PSR J0553+4111) – stars: neutron

1. Introduction

Pulsars are rapidly rotating neutron stars that are known as physics laboratories in extreme conditions with strong magnetic fields. As is well known, the majority of pulsars have very stable rotation periods, at least for a few years. At the same time, most pulsars have stable average pulse profiles. However, it is found that some pulsars exhibit unregular single-pulse emission such as fluctuation in pulse width, pulse phase and pulse intensity (Wen et al. 2016). The phenomenon of single-pulse emission variation in pulsars specifically includes nulling (Backer 1970; Ritchings 1976; Wang et al. 2007; Gajjar et al. 2012; Wen et al. 2016), mode changing (Bartel & Hankins 1982; Wang et al. 2007; Wen et al. 2020; Yan et al. 2020), giant pulses (Staelin & Reifenstein 1968; Hankins et al. 2003; Kuzmin & Ershov 2006; Sun et al. 2021), subpulse drifting (Drake & Craft 1968; Weltevrede et al. 2006, 2007; Basu et al. 2016, 2019; Wen et al. 2022) and so on. The investigation of

single-pulse emission variation will help us to reveal the physical mechanism of emission for radio pulsars.

Mode changing is a type of emission variation where pulsars have two or more emission states, and pulse nulling can be regarded as an extreme mode changing (Wang et al. 2007). Some pulsars have periodic mode changing, such as PSR J1048 −5832, which periodically transforms between strong and weak modes (Yan et al. 2020). Sub-pulse drifting is an emission phenomenon in which pulse components move regularly in phase (Drake & Craft 1968). The sub-pulse drifting phenomenon is explained with the sparking gap model (Ruderman & Sutherland 1975). Many authors (e.g., Gil & Sendyk 2000) further develop this model to account for the variety of sub-pulse drifting. Single-pulse modulation phenomenon refers to the change of pulse energy with time. Nulling is the phenomenon in which observed pulsed emission suddenly disappears and then returns to normal emission on typical

Table 1
Parameters For Two Pulsars

Name	P (s)	DM (pc cm^{-3})	τ (yr)	B_s (G)	Observation Times	Central Frequency (MHz)	Sample Time μs
J0211+4238	0.35	49.7	5.02×10^9	1.99×10^{10}	21	1250	49.152
J0553+4111	0.56	37.9	6.44×10^8	8.88×10^{10}	22	1250	49.152

Note. From left to right, the columns are pulsar name, period (P), dispersion measure (DM), characteristic age (τ), surface magnetic field (B_s), observation time, central frequency and sample time.

timescales ranging from seconds to hours; it usually occurs at all frequencies and all components of a single-pulse (Ritchings 1976; Wang et al. 2007). This phenomenon was first discovered by Backer (Backer 1970). Currently, more than 200 pulsars are known to have nulling (Sheikh & MacDonald 2021). Nulling pulsars can be confirmed by a pulse energy distribution histogram (Wang et al. 2007). Nulling fraction (NF) is a fundamental parameter to describe the degree of emission variation, that is, the ratio of the periods in which emission was not detected to the whole observed duration. For example, PSR J1717−4054 has extreme nulling with an NF of 95% (Wang et al. 2007). The nulls of individual pulsars, for example, PSR J1832+0029, also show varieties in the durations, which range from just several pulses to thousands of pulses (Lorimer et al. 2012). Previous investigations found that the nulling duration follows an exponential distribution and has the characteristics of a random Poisson point process (Gajjar et al. 2012). The NF of pulsars is reported to be related to the pulsar's characteristic age and rotation period (Ritchings 1976; Biggs 1992). In some pulsars, the emission state is not random between null and burst, but periodic, which is called periodic nulling. Periodic nulling has been observed in many pulsars with a large timescale of seconds for PSR J1819 +1305 (Rankin & Wright 2008), hours for PSR B0826−34 (Durdin et al. 1979) and one month for PSR B1931+24 (Kramer et al. 2006). Different modes of transition between null and burst emission states have been observed in some pulsars. For PSR B0818−41 (Bhattacharyya et al. 2010) and PSR J1502−5653 (Li et al. 2012), the pulse energy begins an abrupt rise after null and a gradual decline at the end of the burst state. On the other hand, PSRs B0031−07 and J1738 −2330 exhibit an abrupt null after the burst (Vivekanand 1995; Gajjar et al. 2014). Most transitions of PSR J1727−2739 from null to burst last several pulses, and the transition from burst to null involves both abrupt and gradual pulse energy decline (Wen et al. 2016). Wang et al. (2020) first found details of the transition between null and burst in observations of PSR J1509 +5531. PSR J0901−4046 is an ultra-long-period radio-emitting neutron star with a spin period of 75.88 s; its radio emission has unique spectrotemporal properties, such as quasi-periodicity and partial nulling which provide important clues to the emission mechanism (Caleb et al. 2022). Many years after

the detection of the nulling phenomenon, its emission physical mechanism remains unclear. Several models have been proposed to try to explain the nulling phenomenon, perhaps the cessation of emission in the polar cap region (Ruderman & Sutherland 1975) or the occlusion of an orbital companion (Cordes & Shannon 2008); it could also be caused by instability in the magnetosphere (Geppert et al. 2003).

There are some pulsars with multiple variations of single-pulse emission. Not only nulling but also sub-pulse drifting was detected in PSR J1727−2739 and PSR J1822−2256, moreover PSR J2048−1616 with quasi-periodic nulling also manifests the phenomenon of sub-pulse drifting (Wen et al. 2016; Basu & Mitra 2018; Wang et al. 2021b). Basu et al. (2020) investigated the single pulse emission of the pulsar B2000+40, which shows phase-modulated drifting and periodic nulling in the presence of core emission. This provides an opportunity to investigate whether there is a link between these single-pulse emission variations. In recent years, more and more single-pulse studies using Five-hundred-meter Aperture Spherical radio Telescope (FAST) have been published. Zhang et al. (2019) used FAST to perform single-pulse observations of PSR J1926−0652, and the pulse profile indicated that there were four components with nulling lasting from more than 440 pulse periods. The millisecond pulsar PSR J0621+1002 displays periodic pulse intensity modulation (Wang et al. 2021a). Wen et al. (2022) investigated the single-pulse energy distribution and sub-pulse drifting characteristics of PSR J1631+1252. A study of the newly identified pulsar PSR J1900+4221 discovered by FAST shows that it has an NF of 22% and manifests the mode changing phenomenon (Tedila et al. 2022).

In this paper, we use the FAST data to analyze the single-pulse energy distribution, modulation characteristics and polarization property of the two pulsars and nulling phenomenon of PSR J0211+4235. Section 2 is about observation and data processing, the results are presented in Section 3 and Section 4 provides discussion and conclusion.

2. Observation and Data Processing

We used FAST (Nan et al. 2011) in Guizhou, China to study the single-pulse emission variations of PSRs J0211+4235 and J0553+4111 newly discovered in Commensal Radio

Astronomy FAST Survey (CRAFTS) (Li et al. 2018). FAST is a single antenna radio telescope with three times more sensitivity than Arecibo (Nan & Li 2013). PSRs J0211+4235 and J0553+4111 were discovered on 2018 January 3 and 2017 October 21 respectively by FAST using an ultra wideband receiver, and their single-pulse emission variations have not been reported before. Some parameters for the two pulsars are listed in Table 1. The rotation periods of PSRs J0211+4235 and J0553+4111 are 0.35 s and 0.56 s respectively, and the dispersion measures are 49.7 pc cm^{-3} and 37.9 pc cm^{-3}, respectively. Their characteristic ages are respectively 5.02×10^{9} yr and 6.44×10^{8} yr (Wu et al. 2023). Follow-up observations of PSRs J0211+4235 and J0553+4111 were made using the 19-beam receiver and ROACH2 backend mounted on FAST, with an effective frequency bandwidth of 400 MHz and observation frequency ranging from 1050 to 1450 MHz. The central frequency is 1250 MHz (Jiang et al. 2019), and the observations are from 2020 December to 2021 July. In total, 21 and 22 observation sessions were performed respectively. The time of exposure was about eight minutes on 2021 June 18 for PSR J0211+4235, and each remaining observation lasted four minutes. Each observing session started with a 40 s noise diode measurement for the polarization calibration. The sampling time was 49.152 μs and the data were recorded with full-Stokes polarization in search-mode PSRFITS format 8-bit quantization in 1024 frequency channels with a channel width of 0.488 MHz (Hotan et al. 2004).

We employed DSPSR (van Straten & Bailes 2011) to de-disperse and fold data with the aim to obtain a single-pulse sequence, recorded in PSRFITS format, with 512 phase bins per pulse period. Then, the PAZ and PAZI (Hotan et al. 2004) routines of the PSRCHIVE software package were used to excise radio frequency interference (RFI) and band edge (5% on each side). After the interference was eliminated, all the frequencies and polarizations were scrunched. Since the rotation period of the newly discovered pulsar may be inaccurate, the TEMPO2 (Hobbs et al. 2006) software package was utilized to obtain an accurate pulse period. Each observation eventually produced 684 and 429 single pulses for PSRs J0211+4235 and J0553+4111, respectively. We analyzed energy modulation and fluctuation spectrum using the PSRSALSA software package (Weltevrede et al. 2006).

3. Results

3.1. Single-pulse Sequence

Due to the high sensitivity of FAST, our observations have high signal to noise ratios (SNRs) so that we can deeply investigate the pulsar single-pulse sequence. Figure 1 features the two-dimensional single-pulse stacks of two pulsars and the corresponding average pulse profiles (PSR J0211+4235 on the left and PSR J0553+4111 on the right). The lower panels are single-pulse sequences formed by vertical stacking of single-

pulses one by one. The horizontal and vertical coordinates are pulse phase and pulse number, respectively. The two-dimensional single-pulse stack of PSR J0211+4235 shows more than 600 pulses observed on one epoch, and we can clearly see that there is no emission such as between pulse numbers 800 and 850, and between 1200 and 1300, which is called the pulse nulling phenomenon. From the two-dimensional single-pulse stack of PSR J0553+411, we can see that there are complex variations of pulse energy. It can be seen from Figure 2 that some single-pulses have a higher left peak and some have a higher right peak, showing different intensities. The upper panels are the corresponding average pulse profiles, which are the normalized emission intensity with the phase of the pulse. The profile of PSR J0211+4235 displays a dominant component and a very weak trailing emission. The weak trailing emission intensity is about one-tenth that of the main pulse component, and the width is much wider than the main pulse width. The profile of PSR J0553+4111 consists of two peaks, with the right one being higher, and bridge emission.

3.2. Single-pulse Energy Distribution

We determine the phase of the on-pulse window using the average pulse profile, and then add the phase intensity of the corresponding on-pulse window to get the pulse energy of every single pulse. The on-pulse window is defined as the region in which we see significant pulsed emission over the whole longitude range. For the calculation of off-pulse energy, we choose the same window length as the pulse window length, select the data as smoothly as possible and follow the above method to calculate the off-pulse energy of each single pulse. Finally, on-pulse energy and off-pulse energy are normalized to obtain the normalized pulse energy distribution histogram. The normalized on-pulse energy is obtained by dividing the on-pulse energy per pulse by the average on-pulse energy. Figure 3 displays the normalized pulse energy distribution histogram of the on-pulse window and off-pulse window for these two pulsars (PSR J0211+4235 on the left and PSR J0553+4111 on the right). It can be seen from Figure 3 that the pulse energy distribution of PSR J0211+4235 has two peaks, one of which is at zero energy. The other peak is around its average energy value and there is an overlap between them. The on-pulse energy distribution of PSR J0211+4235 consists of two Gaussian distributions. We can also see that the pulsar has nulling phenomenon. The off-pulse energy distribution presents a Gaussian distribution centered on zero energy which represents the Gaussian random noise contributed by the system temperature. It can be seen from the pulsar energy distribution of PSR J0553+4111 that its on-pulse energy distribution peak is around its average energy value with a Gaussian distribution, and the off-pulse energy distribution peak is at zero energy. In the energy distribution of PSR J0553+4111, there is a small amount of on-pulse
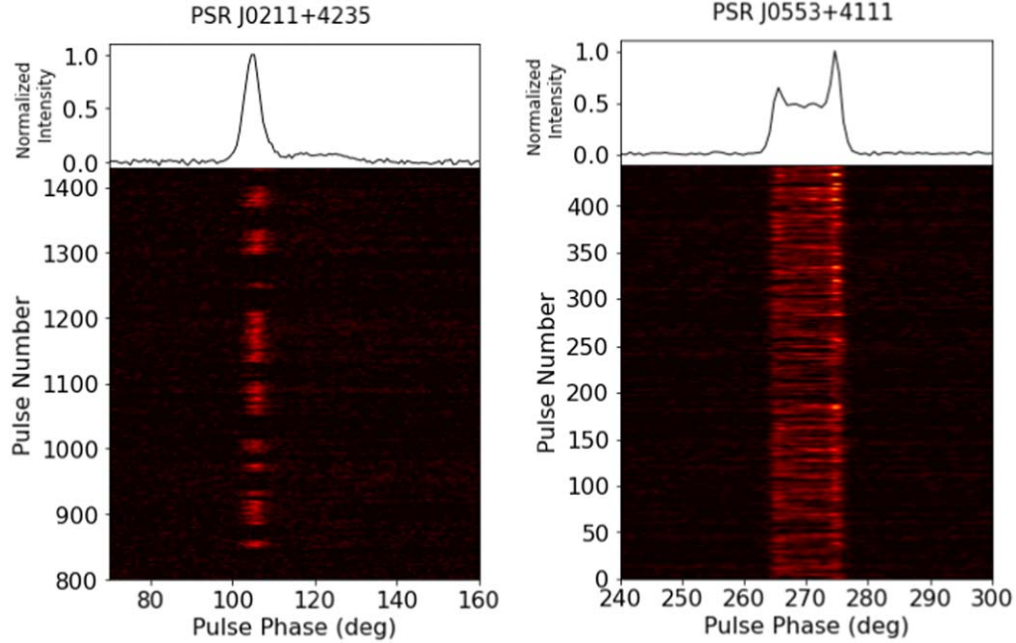
Figure 1. PSRs J0211+4235 (left) and J0553+4111 (right) single-pulse sequences (bottom panels) with pulse number indexed from the observation's start. The top panels depict the average pulse profiles obtained with a whole observing session. J0211+4235 has obvious nulling phenomenon and J0553+4111 has complex emission variations.
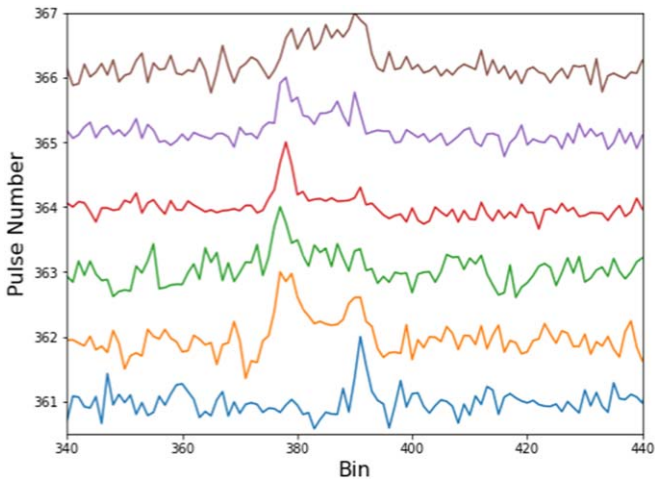

Figure 2. Several single-pulse profiles of PSR J0553+4111.

energy near zero, which we think may be caused by weak emission. The above distributions were all tested by the Kolmogorov–Smirnov (KS) hypothesis test, and the P value was much greater than 0.05.

3.3. Nulling of PSR J0211+4235

From the pulse sequence of PSR J0211+4235, we preliminarily conclude that the emission of PSR J0211+4235

exhibits pulse nulling. The phenomenon of nulling is confirmed in the normalized pulse energy distribution histogram, and the two peaks of the pulse represent null and burst respectively. NF is one of the basic parameters describing the nulling phenomenon. We estimate NF according to the Ritchings (1976) method by subtracting a scaled version of the off-pulse histogram from the on-pulse histogram so that the sum of the different counts in bins with $E < 0$ is zero (Wen et al. 2016). The error of NF is usually calculated by $\sqrt{n_p}/N$, where n_p is the number of null pulses and N is the total number of observed pulses (Wang et al. 2007). The NF of this observation in Figure 3 is $46.1\% \pm 1.8\%$. We use the above method to calculate the NF of 21 observations and obtain a mean NF of $49.2\% \pm 2.4\%$. The NF statistical distribution of 21 observation data is shown in Figure 4. The NF is different due to the short observation duration each time and we can see that NF is mainly distributed between 45% and 55%. There is one session where the NF is above 65%, perhaps because there were just relatively more null pulses recorded during this short observation.

To investigate the characteristics of null and burst, we must first identify the null pulses to distinguish the null state and the burst state. We used the method of Bhattacharyya et al. (2010) to distinguish between null pulses and burst pulses to find two states. The uncertainty of pulse energy is defined as $\sigma_{ep} = \sqrt{n_{on}}\,\sigma_{off}$, where n_{on} represents the length of the selected on-pulse window, and σ_{off} means the root mean square (rms) of
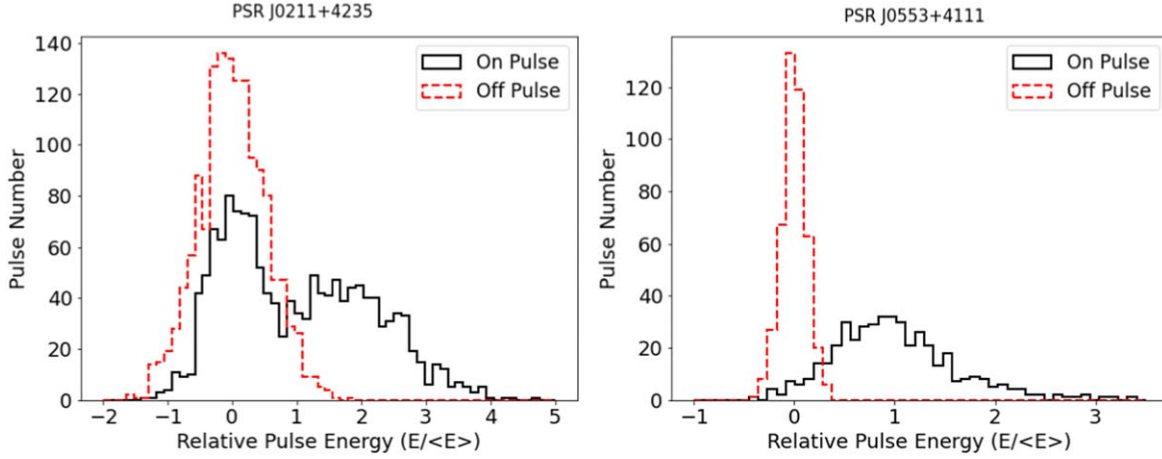
Figure 3. Normalized pulse energy distribution histogram of PSRs J0211+4235 (left) and J0553+4111 (right). The red dashed line represents the off-pulse energy distribution and the black solid line corresponds to the on-pulse energy distribution. The energy is normalized by the average energy.
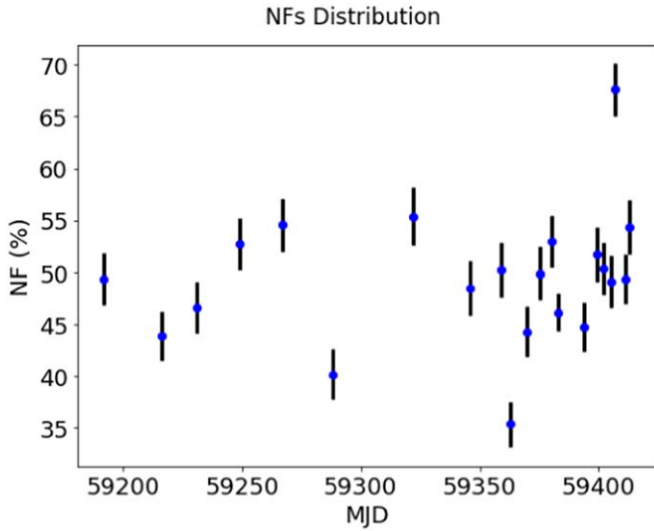

Figure 4. Distribution of NF on different observation dates. The solid blue points represent the NF, and the error bars signify the NF error.

the single pulse off-pulse region. The on-pulse energy is compared with that of σ_{ep}, then the pulses whose energy is less than three times σ_{ep} are classified as null pulses and the rest as burst pulses. Figure 5 depicts the null and burst states of a section of observed single-pulses. In order to identify the state more accurately, we consider two or more nulling pulses or burst pulses as the duration of a timescale. For example, if there is a burst pulse in a continuous nulling pulse, we recognize it as a nulling pulse. A total of 1383 pulses were observed, including 584 null pulses and 799 burst pulses.

We used the above method to identify null pulses and burst pulses of 21 observed data, a total of more than 16,000 pulses, and calculated the duration of the null state and burst state. To identify null and burst more accurately, we checked the pulse sequence with reference to normalized pulse energy and amended the mislabeled pulses. The distributions of recognized null and burst duration are shown in Figure 6. It can be seen from the histogram that the duration of null ranges from 2 to 115 pulse periods, and the duration of burst ranges from 2 to 113 pulse periods. The lengths of the null state and burst state are mainly concentrated in 2–10 pulse periods, indicating that the null and burst of the pulsed variation are frequently between several pulse periods. In the study of the nulling pulsar by others (Wen et al. 2016), the distribution of the nulling duration usually conforms to the power law distribution. The distribution of null length accords with the power law distribution under the short scale of 0–40 pulse periods, and the results are shown in Figure 6.

After identifying the null state and the burst state, we fold all profiles of all null pulses (584 pulses) and burst pulses (799 pulses) to obtain the average pulse profiles of the two states, as displayed in Figure 7. The top panel features the average pulse profile of the burst state. The bottom panel shows the null mean pulse profile, illustrating that there is no significant emission component greater than three times σ. This means that there is no pulse emission in the null state.

The investigation of the transition between the null state and the burst state helps us to understand the different modes of pulse energy change. Figure 8 shows the relative pulse energies of a segment pulse and their corresponding null states or burst states. The abscissa is the number of pulses and the ordinate is the relative pulse energy and states. In several active pulses after the null state, the pulse energy rises relatively abruptly. There are two pulse energy variation modes during the transition from burst state to null state. One, indicated in the first red dashed box, exhibits a gradual decline in pulse energy during variation. The other, outlined in the second red dashed
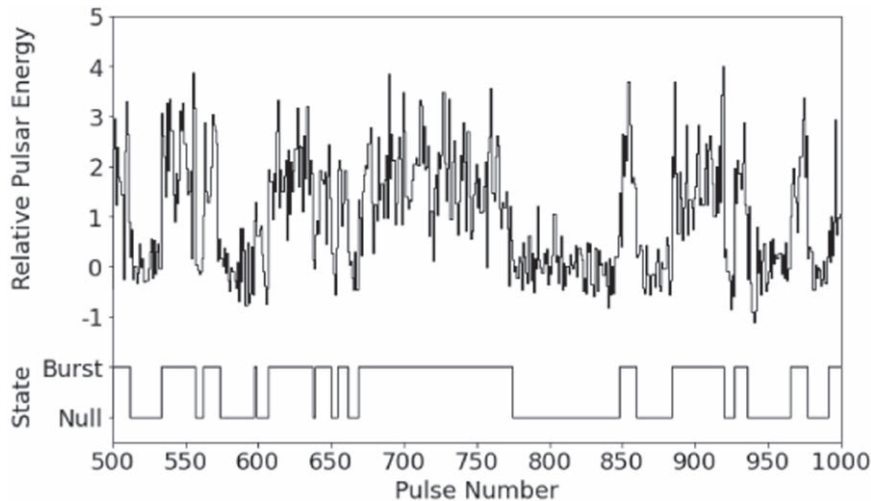
Figure 5. The figure depicts the variation of emission between the 500th pulse and the 1000th pulse. The upper panel presents the relative pulse energy of the selected pulse. The lower panel displays the identified null and burst states.
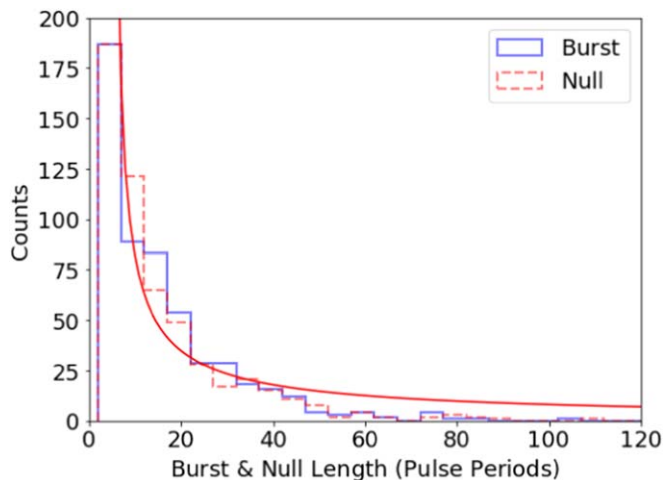

Figure 6. Duration distributions of null (red dashed line) and burst (blue solid line) states. The solid red line in the figure indicates a power law distribution fitted to that of null duration with short scales of 0–40 pulse periods.
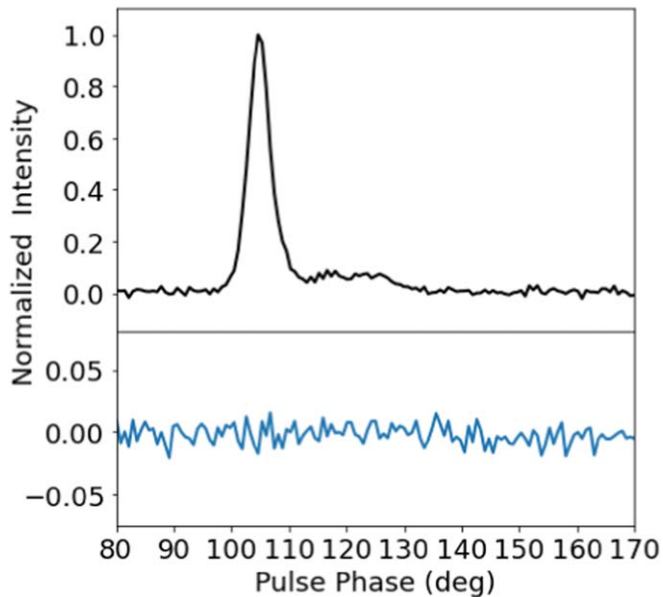

Figure 7. Average pulse profiles for null state (bottom panel) and burst state (top panel).

box, shows a relatively abrupt decline. These two pulse-energy variation modes were also observed on other dates. PSR J0211 +4235 tends to have relatively strong energy in the first few pulses from null state to burst state, which may be caused by the unstable transformation of the magnetospheric structure.

The average pulse profile of the last active pulse (LAP) before nulling differs in shape from that of the first active pulse (FAP) after nulling and many studies about these have been published (Deich et al. 1986; Gajjar et al. 2014; Wen et al. 2016; Rejep et al. 2022). We selected all FAPs and LAPs from 1383 pulse periods. Their average pulse profile is displayed in Figure 9. The peak of FAP (black dashed line) is 0.81, and the peak of LAP (red dash-dotted line) is 0.1 higher than FAP.

They all have a principal pulse component and a weak trailing component, and their pulsed width is the same. The differences observed between the average pulse profile of FAP and LAP suggest that the emission of the pulsar before and after the burst state is changing and the plasma conditions of the surface magnetic field may be different.

To investigate whether the nulling of PSR J0211+4235 is periodic, we used a similar method to Gajjar et al. (2017); Rejep et al. (2022) to process the data. Setting the recognized burst pulse to one and the null pulse to zero, the Fourier
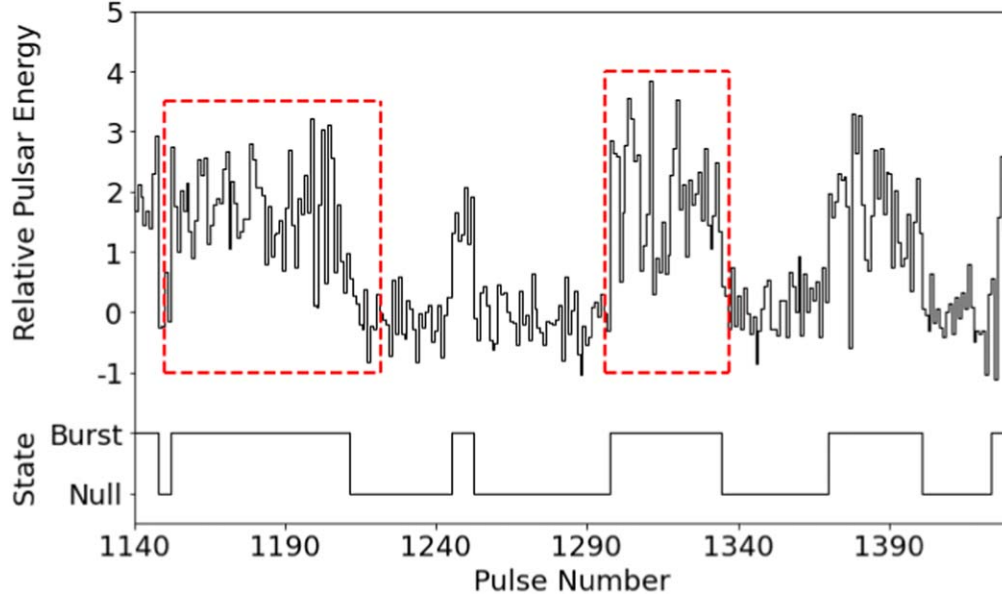
Figure 8. Relative pulse energy variations for 290 pulses (top panel) and transitions between null and burst states (bottom panel).
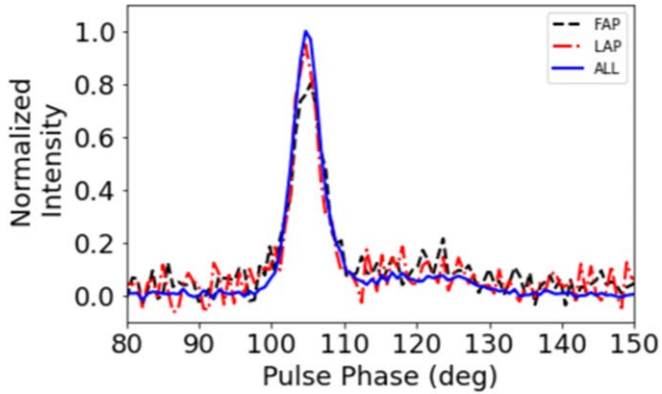

Figure 9. Average pulse profiles of FAP (black dashed line), LAP (red dash-dotted line) and average profile of all bursts (solid blue line).
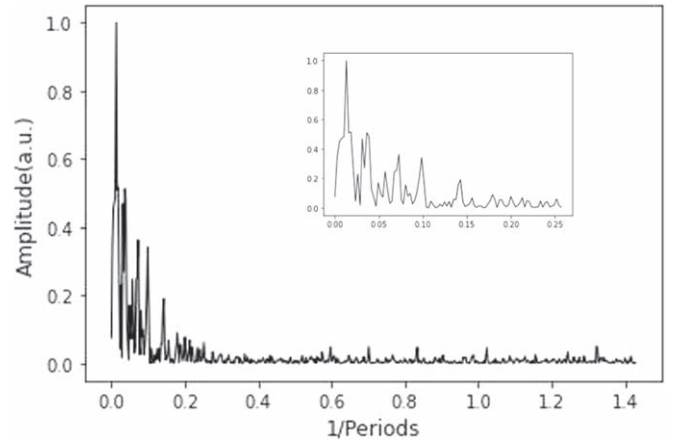

Figure 10. Fourier spectrum of the burst and null states. The inset plot features a zoom in around the strongest spectral feature.

transform is then applied to this set of zeros and ones, and the result is shown in Figure 10. The quasi-period is 76 ± 10 P_0 (P_0 is the pulsar rotation period). We then investigate the change of P_3 over time in one observation. The result is displayed in Figure 11. There are 1383 pulse periods in this observation, and we divide the duration into several segments, where 200 pulses are in one segment, and the seventh segment is 183 pulses. We also count the change of each observed nulling period with time, as shown in Figure 12. It can be seen that the average value is around 70, and the distribution of P_3 is relatively scattered. We think this is due to the short duration of each observation. We find that its periodicity is different in long timescale and short timescale, and P_3 has significant changes.

As for the emission characteristics of PSR J0553+4111, we analyze the data and conclude that this pulsar does not have pulse nulling and mode changing under short-term observations. Although the pulse stack we see shows a variety of more complex pulses, we do not find a regular transformation.

3.4. Single-pulse Modulation

To investigate the single-pulse modulation of each epoch of these two pulsars, we calculated the longitude resolved modulation index distribution, longitude resolved fluctuation spectrum (LRFS) (Backer 1970), and two-dimensional fluctuation spectrum (2DFS) (Edwards & Stappers 2002). The
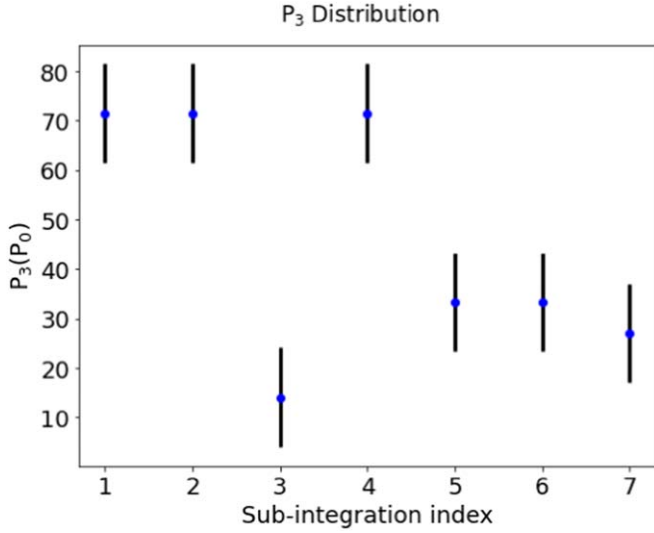
Figure 11. The change of the nulling period with respect to time in one observation. The blue dots with black error bars stand for P_3.
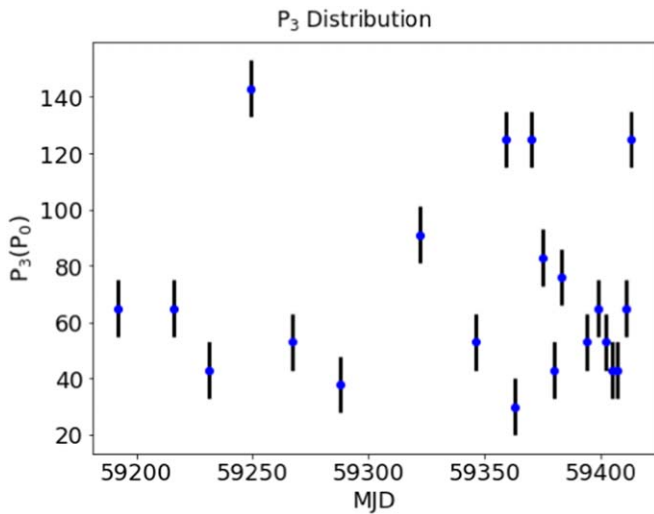

Figure 12. The change of the nulling period with respect to time. The blue dots with black error bars stand for P_3.

longitude resolved modulation index is defined as: $m = \sqrt{\sigma_{\mathrm{on}}^2 - \sigma_{\mathrm{off}}^2}\big/\langle I \rangle$, σ_{on} and σ_{off} are the rms of on-pulse intensity and off-pulse intensity respectively, and I is the on-pulse intensity. Each longitude of the average pulse corresponds to a different modulation index. The magnitude of the modulation index reflects the strength of the pulse intensity variation at a given pulse longitude. The modulation index varies with the phase of the average pulsar profile. LRFS is used to determine whether the pulse intensity varies periodically in the direction of time, and 2DFS is used to analyze whether the single-pulse drifts in the direction of longitude.

The Fast Fourier Transform (FFT) is utilized with the length of the FFT being 128. The longitude resolvable modulation index distribution and LRFS of PSRs J0211+4235 on MJD 59383 (2021 June 18) and J0553+4111 on MJD 59409 (2021 July 14) are plotted in Figure 13. It can be seen that the modulation index near the pulse peak of PSR J0211+4235 is close to one, which indicates that the pulse intensity is relatively stable in the burst state. The modulation index of PSR J0553+4111 is less than one at the two peaks and fluctuates greatly between the two peaks of the pulse profile. The pulse intensity varies greatly in the region with a relatively large modulation index. The vertical frequency axes of LRFS and 2DFS represent P_0/P_3, where P_0 signifies the pulsar rotation period and P_3 means the periodicity of pulse intensity modulation. The horizontal frequency axis of 2DFS corresponds to P_0/P_2, where P_2 stands for the horizontal drifting period of the sub-pulse. For more details on the power spectrum, please see Weltevrede et al. (2006). LRFS analysis indicates that PSR J0211+4235 has intensity modulation in the time direction and the modulation period is $71 \pm 10\ P_0$. This is in accord with the period that we get in subsection 3.3 from the Fourier transform. So, the intensity modulation of J0211+4035 is contributed by periodic nulling. It means the pulse nulling is periodic and the nulling period is $71 \pm 10\ P_0$. As for other epochs, the results are similar. PSR J0553+4111 has no obvious periodic intensity modulation under short-term observation.

We divide the pulse of J0211+4235 into separate parts of the main component and the weak component, and investigate the periodicity of variation of each component sequence by using a Fourier transform. The result on MJD 59383 (2021 June 18) for PSR J0211+4235 is displayed in Figure 14, which affirms that the main component sequence has a periodic energy variation of $73 \pm 10\ P_0$. It is close to the nulling period, indicating that the periodicity of the main component variation dominates the periodicity of energy modulation. For the weak component, there is no apparent periodicity, which may be caused by the weak faint flux of this component. For the pulsar J0553+4111, we divide its pulse into three components: the left component, the middle component and the right component. The periodicity of energy change is examined by the Fourier transform of the energy of the three component sequences. The result on MJD 59409 (2021 July 14) for J0553+4111 is featured in Figure 14, with the left component showing quasi-periodic modulation of $125 \pm 10\ P_0$. The other components have no obvious periodicity.

The 2DFS on MJD 59383 (2021 June 18) for PSR J0211 +4235 and that for PSR J0553+4111 on MJD 59409 (2021 July 14) for PSR J0553+4111 is shown in Figure 15. It can be clearly seen from the figure that P_0/P_2 is 0 at the peak. This indicates that there is no sub-pulse drifting phenomenon in the short-time observation of these two pulsars.
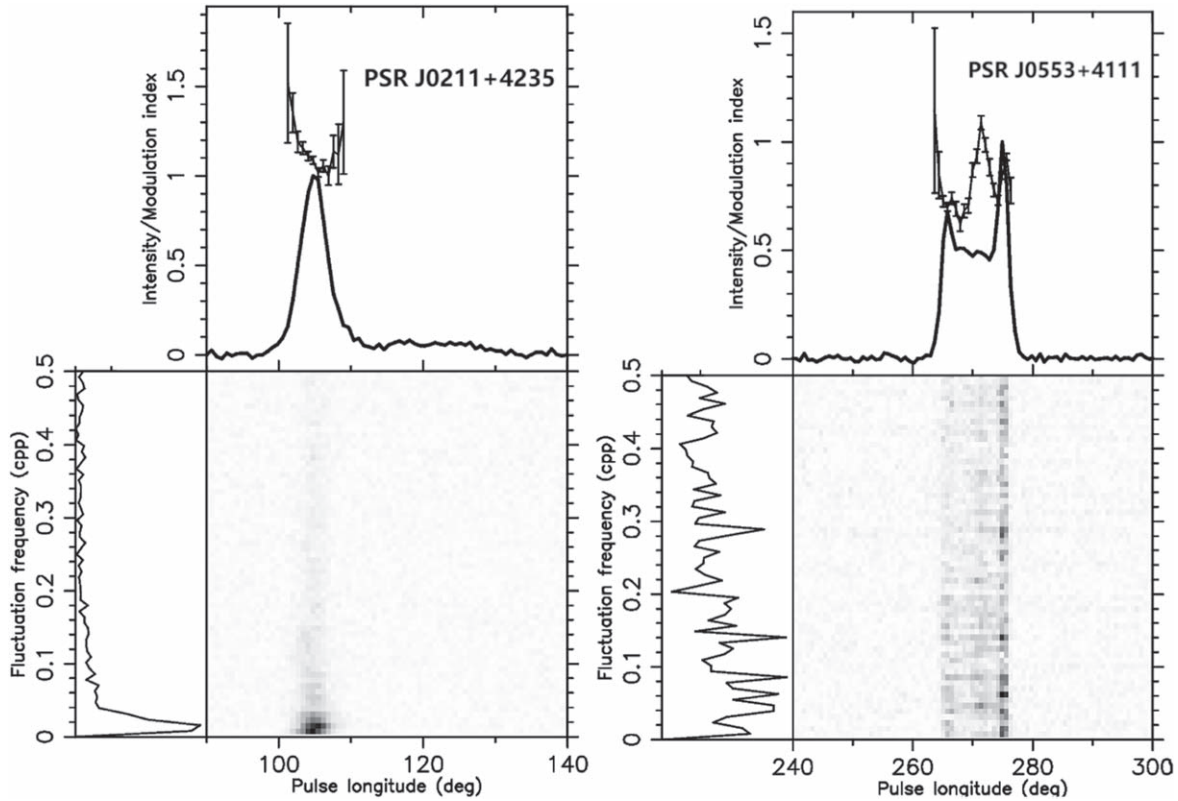
Figure 13. Longitude resolved modulation index distributions (top panel) and LRFS (vertical solid line on the left side of each figure) for PSRs J0211+4235 (left) and J0553+4111 (right).
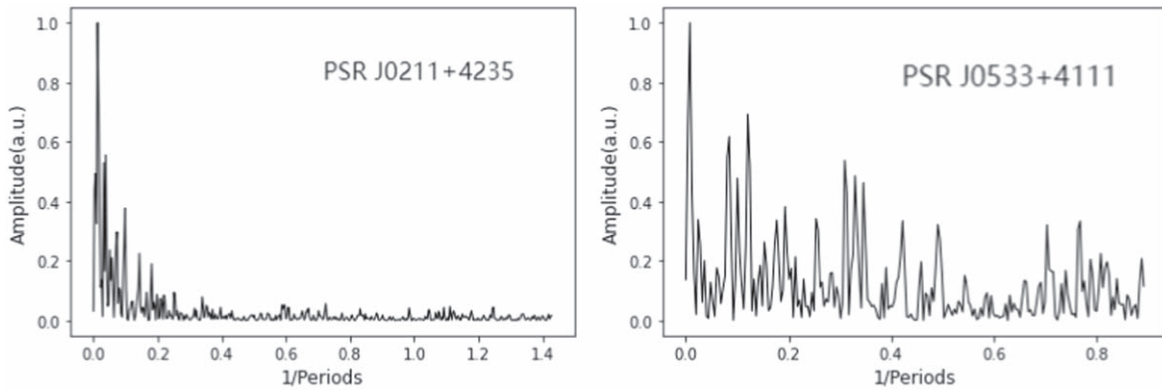

Figure 14. Fourier transform of the energy of J0211+4235 main component sequence (left panel) and J0553+4111 left component sequence (right panel).

3.5. Polarization Characteristics

For the sake of studying the polarization characteristics of pulsars, we first use PSRCHIVE to perform polarization calibration on the observed data. Then the polarization profile of the pulsar is drawn. We calculate the rotation measurement (RM) of the Earth's ionosphere for each observation after the best Faraday RM was obtained by RMFIT. The fitting RM of the pulsar minus the RM of the Earth's ionosphere gives the true RM of the pulsar and yields the changes of the RM of the two pulsars over time, as shown in Figure 16. We can see from the figure that the change of RM does not vary much and fluctuates around a fixed value. The RMs of PSRs J0211+4235 and J0553+4111 are 46(17) rad m^{-2} and −16(14) rad m^{-2}, respectively, where the contribution of the Earth's ionospheric Faraday rotation (Sotomayor-Beltran et al. 2013) is taken out.

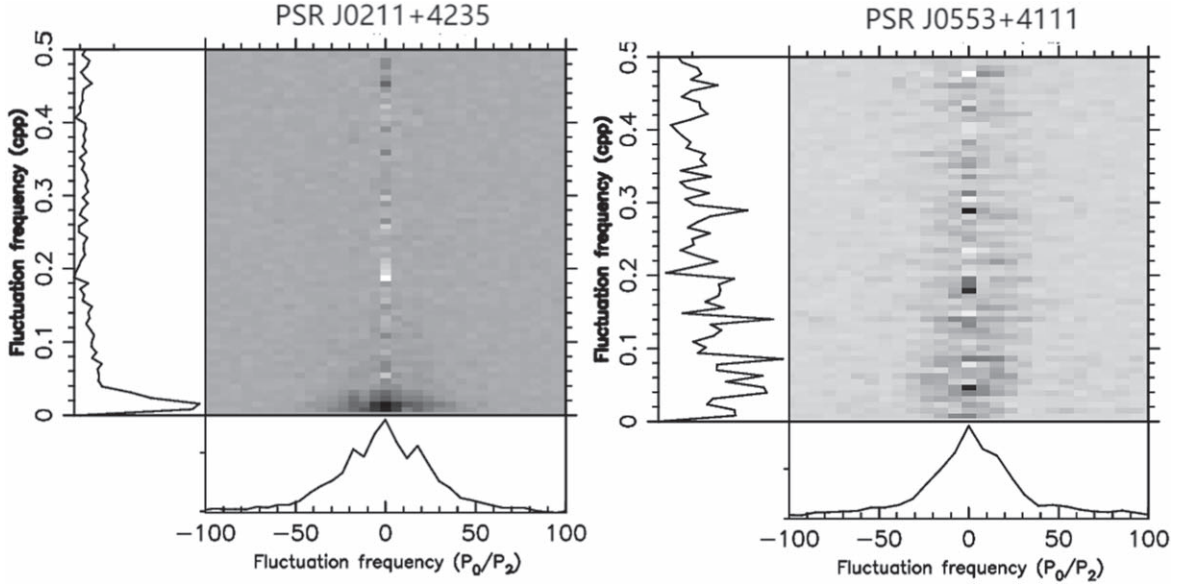**Figure 15.** 2DFS of PSRs J0211+4235 (left) and J0553+4111 (right), with horizontal solid lines P_0/P_2 at the bottom and P_0/P_3 perpendicular at the left.

We superimpose all the polarization results obtained by observation, and the pulse polarization profile obtained is shown in Figure 17. The polarization of pulsar emission is measured as four Stokes parameters, namely I, Q, U and V. The linear polarization is described by $L = \sqrt{(Q^2 + V^2)}$ and V is the circular polarization. For PSR J0211+4235, the distribution of polarization Position Angle (P.A.) corresponding to the weak pulse following the main pulse is higher than that of the main pulse and is relatively smooth; the polarization P.A. curve of the main pulse is S-shaped. The linearly polarized profile of PSR J0553+4111 is lower at the two peaks of the pulse and higher in the middle. Most other pulsars have linearly polarized profiles similar to pulse profiles; it seems that the linearly polarized profile of PSR J0553+4111 is strange. This pulsar has obvious depolarization at the edge of its profile. The percentages of linear polarization are 14.42% and 30.32% respectively. The percentages of circular polarization are 9.88% and 22.79% respectively. It is noted that the circular polarization is reverse for the first half, and we calculate the absolute value. We use the same method as Rankin (1990) to calculate the pulsars' magnetic inclination angle using a pulse width of 50% intensity (Maciesiak et al. 2011; Tedila et al. 2022). The magnetic inclination angles α of PSR J0211+4238 and PSR J0553+4111 are about $65°.12$ and $20°.18$, respectively.

4. Discussion and Conclusions

4.1. Discussion

The dominant duration of nulling is short for PSR J0211+4235, which is demonstrated by the histogram of null lengths

with a peak at the lowest bin. It has been argued that the short-duration nulls are related to stochasticity in the emission process while the large-scale changes in the magnetosphere lead to the longer-duration nulls (Cordes 2013). More than half of the nulling pulsars exhibit NF of 10% (Wang et al. 2020). For PSR J0211+4235, it has an NF of 49%, which is relatively high and roughly consistent among observations. NF is reported to be related to the age or rotation period of the pulsar with a positive correlation (Ritchings 1976; Biggs 1992; Wang et al. 2007). Normal pulsars with large ages are apt to show large NFs with a correlation coefficient of 0.33 (Wang et al. 2020). Interestingly, Sheikh & MacDonald (2021) found NF's weak dependency on pulse width, as well as a weak correlation between NF and spin period which could be ascribed to selection effects.

A power law relation of the pulse width with the period is presented with $W_{10} = (14.2 \pm 0.4)°(P/s)^{\mu}$ where $\mu = -0.29 \pm 0.03$ is obtained by Posselt et al. (2021). As for J0211+4235, the observed pulse width is larger than the inferred pulse width. The measurement of J0553+4111's pulse width is in accord with the estimated pulse width. The pulsar pulse width usually decreases with an increasing period. The slowest spinning pulsars have the narrowest pulse widths. In our two sources, the pulsar with a large period has a small pulse width.

To investigate how the pulse width varies with frequency, we divide the observed data into two subbands. Then the center frequency of these two subbands is 1125 MHz and 1375 MHz respectively. The W_{50} of PSR J0211+4238 is $4°.4 \pm 0°.7$ and $4°.6 \pm 0°.7$ respectively at 1125 and 1375 MHz. Another pulsar, J0553+4111, has pulse widths at these two frequencies of
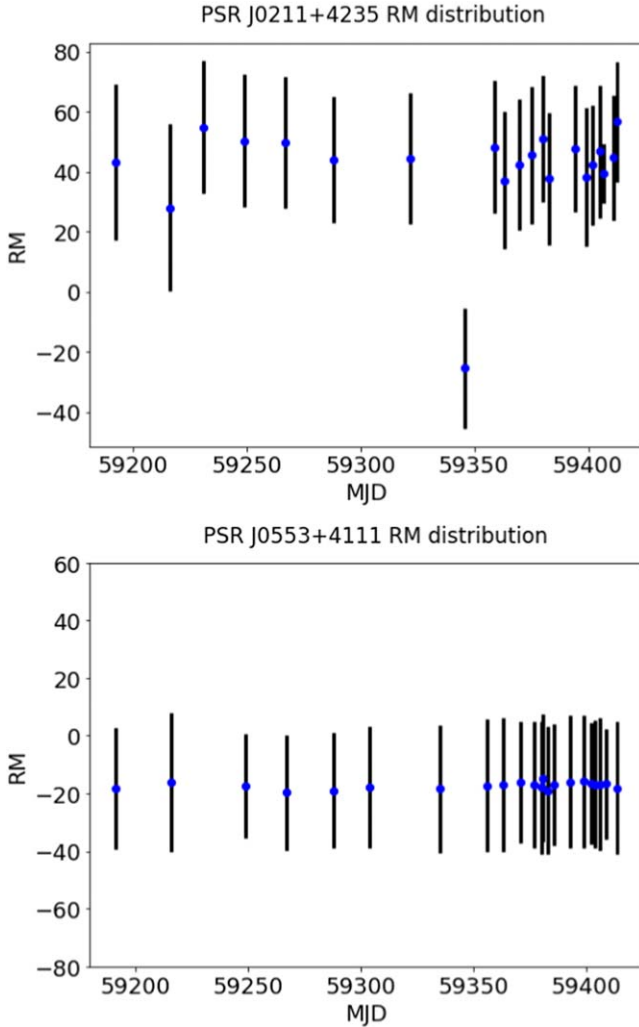
Figure 16. The distribution of RM over time for PSRs J0211+4235 (left) and J0553+4111 (right). The blue dots with black error bars stand for RM.

$10°.9 \pm 0°.5$ and $10°.8 \pm 0°.4$. The pulse profiles at 1125 and 1375 MHz were presented in Figure 18 for comparison. We can see that the pulse profile of J0211+4235 at 1375 MHz is wider than that of 1125 MHz, and the weak pulse component is also stronger. For J0553+4111, the change in its width is not obvious in Figure 18, but the change in the middle component is significant. According to the RS model, the lower the observation frequency is, the larger the pulse width becomes. The pulse width of J0553+4111 does not change obviously with frequency. The observed pulse width of J0211+4238 increases with frequency. Rankin calls this the "absorption" phenomenon (Rankin 1983b).

The average pulse profiles of pulsars have diverse shapes, such as unimodal, bimodal, trimodal and complex multimodal. This shows that the emission intensity distribution of the pulsar emission region is relatively complicated. For different pulsars,

their emission region structure is not identical. The average pulse profile of the pulsar is the emission intensity obtained when the observer's line of sight sweeps across the emission beam of the pulsar. While the line of sight sweeps through different positions in the emission beam, the contour obtained may be different, which reflects the one-dimensional emission information on the emission region. For two-dimensional information on the pulsar emission region, researchers have put forward several empirical models after analyzing a large number of pulsar profiles. By analyzing the average pulse profile of dozens of pulsars, Backer (1976) proposed an empirical model of "core + hollow cone" according to the analysis results. In this model, the average pulse profile is classed as single peak, double resolved peaks, or double unresolved peaks, triple peaks and multi-peak. This was the first time the existence of the core component was proposed. A few years later, Rankin proposed the "core + cone" structure model based on the polarization and average pulse profile of the pulsars. This model consists of a middle core structure and two hollow cones nested on the core structure. The emission regions in the hollow cone display a disjointed patch structure (Rankin 1983a). For the pulsar PSR J0211+4235, the analysis of the polarization P.A. shows that the main pulse and the following faint component together can be regarded as a double peak profile. As the P.A. is almost constant across the trailing component, and has significant gradient across the main component, this pulsar likely accords with the beam model of the "core + partial cone," where the conal emission is weak. According to the average pulse profile and polarization image of PSR J0553+4111, the pulsar beam has possibly the form of "core + cone," owing to the large rate of swing near the pulse center.

We compared these two pulsars we studied with other pulsars observed by FAST in recent years. Also for the new pulsars discovered by FAST, PSR J1631+1252 is a pulsar with a rotation period of 0.31 s, which is a little shorter than the period of 0.35 s for PSR J0211+4235. These two pulsars have very close rotation periods; the average pulse profiles are also similar in this way that the main pulses are followed by weak radiations, but their emission characteristics are quite different. PSR J1631+1252 has the phenomenon of sub-pulse drifting, which is almost continuous in the pulse train and does not have the phenomenon of nulling. PSR J0211+4235 is older than PSR J1631+1252 and has the phenomenon of nulling, which supports that nulling is correlated with pulsar age, but the pulse component of J0211+4235 has no regular change in phase. Admittedly, there are many pulsars that possess both pulse nulling and sub-pulse drifting simultaneously. We still need to investigate more pulsars to study whether the sub-pulse drifting phenomenon is related to the pulse nulling. Comparing PSR J0211+4235 with PSR J1900+4221, both pulsars have obvious nulling phenomenon, and the NF of the former is almost twice that of the latter (Tedila et al. 2022). As PSR
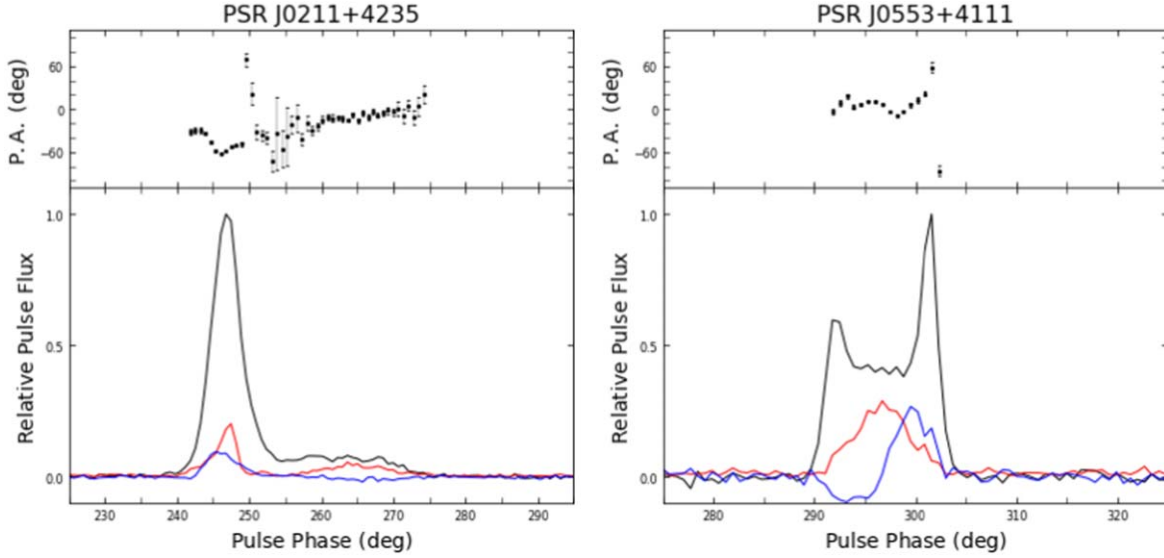
Figure 17. Polarization profiles of PSRs J0211+4235 (left) and J0553+4111 (right). The black, red and blue solid lines are the total intensity, linear polarization intensity and circular polarization intensity respectively. The black dots with error bars in top panels are the polarization P.A.s.

J1900+4221 is younger than PSR J0211+4235 and has a longer period of 4.341 s, it supports the hypothesis that NF is correlated with pulsar age. The pulsar PSR J1926−0652 observed by FAST also has nulling phenomenon, and its NF is relatively high, 75%. The pulsar also has sub-pulse drifting, which is complicated by the fact that its profile has four components, each with its own drifting (Zhang et al. 2019). We plotted the new nulling pulsars discovered by FAST in the P-$\dot{P}$ diagram shown in Figure 19. It looks like the FAST newly discovered nulling pulsars are possibly relatively old pulsars or long period pulsars.

Several models have been proposed to explain pulsed nulling. Timokhin (2010) suggested that the magnetosphere possesses changed states, such as different geometric states or different electron distributions. The magnetosphere can switch between these states, where nulling is caused when a new beam is outside of the line of sight or no radio emission is produced. There is also a hypothesis that nulling is attributed to the cessation of emission in the polar cap region (Ruderman & Sutherland 1975) or the occlusion of an orbital companion (Cordes & Shannon 2008). Some models suggest that pulse nulling is caused by changes in emission mechanism (Zhang et al. 1997) and loss of line of sight (Herfindal & Rankin 2007). Other models suggest that pulse nulling is due to the temporary loss of radio emission associated with the generation of pole-gap plasma (Filippenko & Radhakrishnan 1982). It has also been suggested that it may be caused by changes in the magnetic structure of the polar cap (Geppert et al. 2021). Dyks (2021) argued that the viewing of a radio beam gives rise to the pseudo-chaotic complexity of single pulses, where the sporadic nulling is caused by the drifting azimuthal zones of the beam.

Olszanski et al. (2022) proposed that an evolution in the pair formation geometries produces core/conal emission and other emission effects, for instance nulling and mode-changing.

4.2. Conclusion

In this paper, we report for the first time the single-pulse emission variations of the newly discovered PSRs J0211+4235 and J0553+4111 from the CRAFTS program. From the normalized single-pulse energy distribution, we can prove that PSR J0211+4235 has pulse nulling and we calculated the mean NF of 21 observations to be 49.2% ± 2.4%. The pulses of these two states are mainly concentrated in 2–10 pulse periods, which means that the transition between burst and null is very frequent. We see a variety of energy changes during the transition between burst and nulling. The pulse energy rises abruptly from null to burst but decreases abruptly and gradually from burst to null. Analysis of FAP and LAP revealed differences in their average pulse profiles, suggesting that the emission of the pulsar before and after the burst state is changing. For the periodicity of pulsed null, we obtain a quasi-period of $71 \pm 10 P_0$. PSR J0553+4111 had a multiple component profile and the single-pulse emission varied complexly.

We investigated their longitude resolvable modulation index distributions. The results show that PSR J0211+4235's pulse energy varied stably in the burst state. The modulation index of the middle components of PSR J0553+4111 pulse changes greatly, and the pulse intensity changes greatly where the modulation index is relatively large. Its pulse energy varied wildly. Through LRFS, it can be obtained that PSR J0211
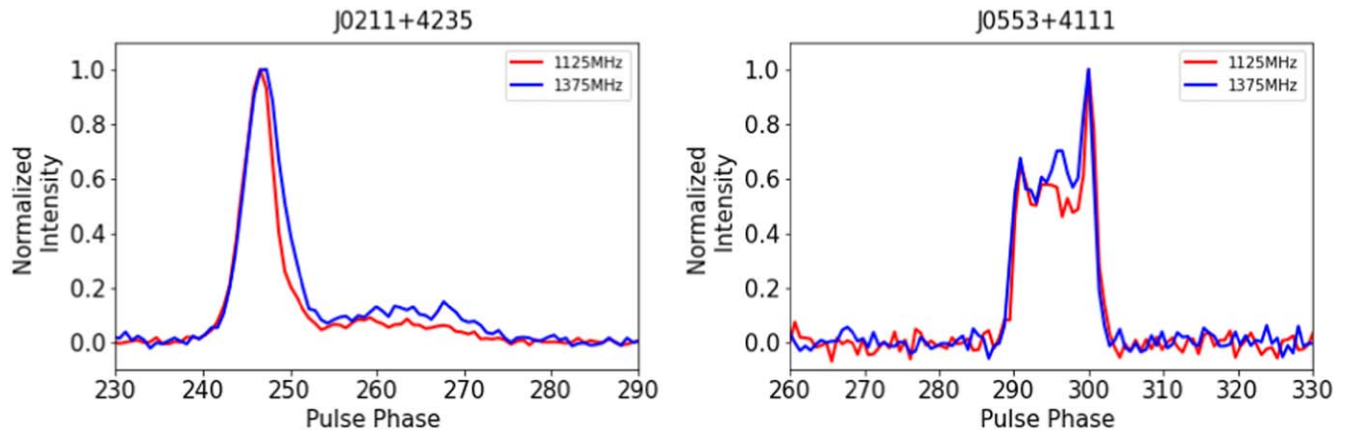
Figure 18. The pulse profiles at 1125 MHz and 1375 MHz of PSRs J0211+4235 (left) and J0553+4111 (right).
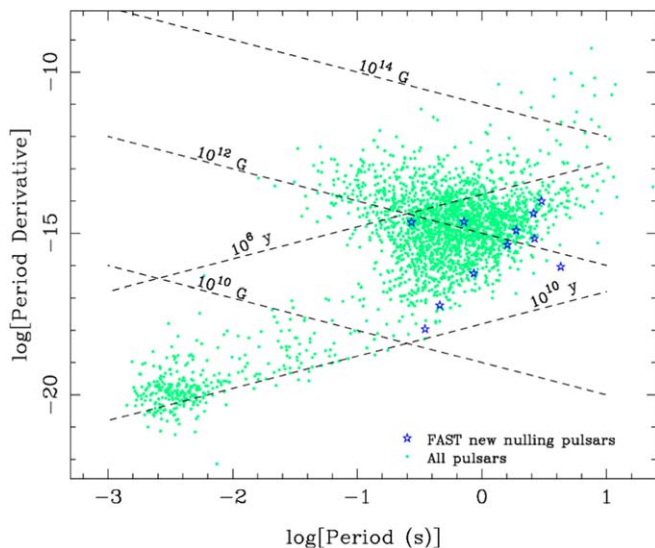

Figure 19. A $P\text{-}\dot{P}$ diagram. The lines represent the pulsar's characteristic age and the strength of its surface magnetic field.

+4235 has intensity modulation. Neither pulsar has the phenomenon of sub-pulse drifting.

It is not clear how variations in the magnetosphere on the pulsar surface affect the modulation of the pulsar emission intensity. A more accurate nulling period and NF of PSR J0211+4235 can be determined by longer exposure time observations, so as to better study the essential cause of the nulling phenomenon. In addition, observations with a long time of exposure can also be used to investigate whether PSR J0553+4111 has mode changing phenomenon and modulation periodicity.

Acknowledgments

Data Availability

Raw data are released by the FAST data center and can be accessed through it. Reduced data products are available upon reasonable request.

ORCID iDs

Zhigang Wen ◉ https://orcid.org/0000-0003-2991-7421
Mengyao Xue ◉ https://orcid.org/0000-0001-8018-1830
Wenming Yan ◉ https://orcid.org/0000-0002-7662-3875
Jiarui Niu ◉ https://orcid.org/0000-0001-8065-4191

References

Backer, D. C. 1970, Natur, 228, 42
Backer, D. C. 1976, ApJ, 209, 895
Bartel, N., & Hankins, T. H. 1982, ApJL, 254, L35
Basu, R., Lewandowski, W., & Kijak, J. 2020, MNRAS, 499, 906
Basu, R., & Mitra, D. 2018, MNRAS, 476, 1345
Basu, R., Mitra, D., Melikidze, G. I., et al. 2016, ApJ, 833, 29
Basu, R., Mitra, D., Melikidze, G. I., & Skrzypczak, A. 2019, MNRAS, 482, 3757
Bhattacharyya, B., Gupta, Y., & Gil, J. 2010, MNRAS, 408, 407
Biggs, J. D. 1992, ApJ, 394, 574
Caleb, M., Heywood, I., Rajwade, K., et al. 2022, NatAs, 6, 828

Cordes, J. M. 2013, ApJ, 775, 47
Cordes, J. M., & Shannon, R. M. 2008, ApJ, 682, 1152
Deich, W. T. S., Cordes, J. M., Hankins, T. H., & Rankin, J. M. 1986, ApJ, 300, 540
Drake, F. D., & Craft, H. D. 1968, Natur, 220, 231
Durdin, J. M., Large, M. I., Little, A. G., et al. 1979, MNRAS, 186, 39P
Dyks, J. 2021, A&A, 653L, 3
Edwards, R. T., & Stappers, B. W. 2002, A&A, 393, 733
Filippenko, A. V., & Radhakrishnan, V. 1982, ApJ, 263, 828
Gajjar, V., Joshi, B. C., & Kramer, M. 2012, MNRAS, 424, 1197
Gajjar, V., Joshi, B. C., & Wright, G. 2014, MNRAS, 439, 221
Gajjar, V., Yuan, J. P., Yuen, R., et al. 2017, ApJ, 850, 173
Geppert, U., Basu, R., Mitra, D., Melikidze, G. I., & Szkudlarek, M. 2021, MNRAS, 504, 5741
Geppert, U., Rheinhardt, M., & Gil, J. 2003, A&A, 412, L33
Gil, J. A., & Sendyk, M. 2000, ApJ, 541, 351
Hankins, T. H., Kern, J. S., Weatherall, J. C., & Eilek, J. A. 2003, Natur, 422, 141
Herfindal, J. L., & Rankin, J. M. 2007, MNRAS, 380, 430
Hobbs, G. B., Edwards, R. T., & Manchester, R. N. 2006, MNRAS, 369, 655
Hotan, A. W., van Straten, W., & Manchester, R. N. 2004, PASA, 21 302
Jiang, P., Yue, Y., Gan, H., et al. 2019, SCPMA, 62, 959502
Kramer, M., Lyne, A. G., O'Brien, J. T., Jordan, C. A., & Lorimer, D. R. 2006, Science, 312, 549
Kuzmin, A. D., & Ershov, A. A. 2006, AstL, 32, 583
Li, D., Wang, P., Qian, L., et al. 2018, IMMag, 19, 112
Li, J., Esamdin, A., Manchester, R. N., Qian, M. F., & Niu, H. B. 2012, MNRAS, 425, 1294
Lorimer, D. R., Lyne, A. G., McLaughlin, M. A., et al. 2012, ApJ, 758, 141
Maciesiak, K., Gil, J., & Ribeiro, V. A. R. M. 2011, MNRAS, 414, 1314
Nan, R., & Li, D. 2013, MSEng, 44, 012022
Nan, R., Li, D., Jin, C., et al. 2011, IJMPD, 20, 989

Olszanski, T., Rankin, J., Venkataraman, A., & Wahl, H. 2022, MNRAS, 517, 1189
Posselt, B., Karastergiou, A., Johnston, S., et al. 2021, MNRAS, 508, 4249
Rankin, J. M. 1983a, ApJ, 274, 333
Rankin, J. M. 1983b, ApJ, 274, 359
Rankin, J. M. 1990, ApJ, 352, 247
Rankin, J. M., & Wright, G. A. E. 2008, MNRAS, 385, 1923
Rejep, R., Wang, N., Yan, W. M., & Wen, Z. G. 2022, MNRAS, 509, 2507
Ritchings, R. T. 1976, MNRAS, 176, 249
Ruderman, M. A., & Sutherland, P. G. 1975, ApJ, 196, 51
Sheikh, S. Z., & MacDonald, M. G. 2021, MNRAS, 502, 4669
Sotomayor-Beltran, C., Sobey, C., Hessels, J. W. T., et al. 2013, ionFR: Ionospheric Faraday rotation, Astrophysics Source Code Library, ascl:1303.022
Staelin, D. H., & Reifenstein, E. C. I. 1968, Science, 162, 1481
Sun, S. N., Yan, W. M., & Wang, N. 2021, MNRAS, 501, 3900
Tedila, H. M., Yuen, R., Wang, N., et al. 2022, ApJ, 929, 171
van Straten, W., & Bailes, M. 2011, PASA, 28, 1
Vivekanand, M. 1995, MNRAS, 274, 785
Wang, N., Manchester, R. N., & Johnston, S. 2007, MNRAS, 377, 1383
Wang, P. F., Han, J. L., Han, L., et al. 2020, A&A, 644, A73
Wang, S. Q., Wang, J. B., Wang, N., et al. 2021a, ApJ, 913, 67
Wang, Z., Wen, Z. G., Yuan, J. P., et al. 2021b, ApJ, 923, 259
Weltevrede, P., Edwards, R. T., & Stappers, B. W. 2006, A&A, 445, 243
Weltevrede, P., Stappers, B. W., & Edwards, R. T. 2007, A&A, 469, 607
Wen, Z. G., Wang, N., Yuan, J. P., et al. 2016, A&A, 592, A127
Wen, Z. G., Yan, W. M., Yuan, J. P., et al. 2020, ApJ, 904, 72
Wen, Z. G., Yuan, J. P., Wang, N., et al. 2022, ApJ, 929, 71
Wu, Q. D., Yuan, J. P., Wang, N., et al. 2023, MNRAS, 522, 5152
Yan, W. M., Manchester, R. N., Wang, N., et al. 2020, MNRAS, 491, 4634
Zhang, B., Qiao, G. J., Lin, W. P., & Han, J. L. 1997, ApJ, 478, 313
Zhang, L., Li, D., Hobbs, G., et al. 2019, ApJ, 877, 55